LAB-SCALE EXPERIMENTAL VALIDATION OF A PIEZOELECTRIC ENERGY HARVESTING LAG DAMPER

P. H. de Jong, R. Loendersloot, A. de Boer, P. J. M. van der Hoogt

Structural Dynamics and Acoustics,
Faculty of Engineering Technology,
University of Twente,
Enschede, Netherlands
Email: p.h.dejong@utwente.nl

July 23, 2012

Abstract

Currently the lifespan of helicopter rotor blades is determined based on a conservative lifetime calculation. This leads to blades being discarded while they still possess a significant residual amount of flight-hours. Blade health monitoring systems are desired to actively track the strains in the blade as a means to determine the residual life of the blade, significantly extending the technical life expectancy. A major drawback is the need for an electrical infrastructure to transmit all the signals to and from the rotor hub to the aircraft body. It would be advantageous if the required power could be generated locally.

Within the European Clean Sky project vibration-based power harvesting is chosen as a solution to powering in-blade health monitoring systems. In this paper simulations of a new power harvesting concept are validated experimentally. Local generation of power will allow for a 'plug and play' rotor blade and signals may be logged or transmitted wirelessly to the body of the aircraft. Examples are the blade strains, hinge forces, vibrations and so on.

At the ERF2011 [1] presented a simulation model to predict the electrical output of a lag damper augmented with a piezoelectric based energy harvester. Simulations indicated that for an 8.15m blade the output is to be around 5W. The concept includes a piezo electric stack mounted in the damper rod and in series with the damping element. All forces generated by the damper are also passed through the stack and through the piezo electric effect electric charge is generated. Through the use of advanced circuits the power is conditioned and can be stored in a large capacitor or battery located in the rotor hub.

The concept is validated in the lab. The setup consists of a large stroke shaker delivering a high force at low frequency. A piezoelectric stack with a large pre-stress is used so that it can also cope with the tensile forces generated by the damper. A viscous damper which has no dead zone upon reversal of the motion is used to mimic the lag damper. Although the damper does not possess a similar damping profile as an actual lag damper this does not pose a problem as the peak force is more important than the exact profile. Lastly a laser vibrometer, a force sensor, a thermocouple and a voltmeter are utilized to log relevant data through a SigLab system.

A number of experiments are conducted to verify the simulation model. Following individual component experimentation, different electrical circuits are coupled to the stack and each result is then compared to a simulation of the respective electrical configuration. Two circuits are to be validated: Direct Current Impedance Matching is used as it is a passive circuit and the 'standard' for power harvesting and Synchronous Switch Harvesting on Inductor is used as it is shown to be the best performing circuit investigated in previous simulations [2].

The desired end result is an experimentally validated simulation model of the lag damper - harvester model which can be used to predict power output of similar power harvesting systems.

1. INTRODUCTION

Helicopter rotor blades are critical components of a rotor craft and structural integrity is paramount for the safety of the vehicle. Generally these blades are replaced based on a highly conservative lifetime calculation. The ability to extend the life of these blades would allow for a significant reduction in running costs. The environmental impact would also be decreased due to the significant reduction in materials and fabrication.

Increasing the technical lifespan of the blade will require health monitoring systems to be installed which can keep track of the mechanical loads imposed on the rotor blades. With actual strain data residual lifetime calculations may be performed regularly and the blades can be replaced when they have truly reached the end of their technical lifespan.

A major challenge with such systems is providing sufficient and stable power. Within the European Clean Sky program a number of options have been explored. An inductive generator positioned around the rotor has been deemed unsuitable due to alignment requirements between rotor and body. Slip rings bring high maintenance and an unstable power supply. Power harvesting is also under consideration as an alternative and it will show to be a viable option.

In [2] an investigation was done towards the adaptation of a lag damper to double as a power supply. This device dampens in-plane blade oscillations in rotor craft in order to suppress air and ground resonance. A number of circuits were investigated and the SSHI circuit [3] proved to be the most promising. In [1] some design implications are also investigated in order to maintain correct operation of the lag damper.

This paper reports on the validation efforts undertaken so far to confirm the predictions of the simulations and to improve the feasibility of the concept. The mechanical setup is elaborated on first, followed by a brief discussion of the employed circuitry. Results are presented and discussed and conclusions are drawn.

2. EXPERIMENTAL SETUP

The experimental setup is shown schematically in figure 1. Going from right to left in the figure, the setup consists of a large Bruël & Kjaer shaker equipped with a 4819 shaker head. The shaker is connected to a B&K 8001 impedance head via a rod flexure to mitigate alignment errors. The piezo element is a PiezoMechanik PSt150/3.5$\times$3.5/20 stack in an upgraded housing with 400N preload. Next a viscous damper by ACE Stossdämpfer is used, model HBS-28-50, with a 50mm stroke. It is selected due to its ability to damp in both directions without any free stroke upon reversal. The damper is modified by adding a large aluminium heatsink, manufactured locally, to provide better temperature stability. Other relevant data is given in table 1.

Table 1: Mechanical properties of the experimental setup

	Symbol	Value	Unit
Stack capacitance	C_p	0.96	[μF]
Stack stiffness	k_p	$25{\cdot}10^6$	[N/m]
Piezoelectric coefficient	θ	1.05	[N/V]
Mass shaker core	M	0.9	[kg]
Rod flexure axial stiffness	k_r	$13\cdot10^6$	[N/m]
Electromechanical coupling	k_e^2	0.042	[-]

Not shown in figure 1 is the thermocouple which is used to measure the temperature. Also, the shaker head velocity is measured using a PolyTec laser vibrometer. Data acquisition is done using a SigLab model 20-42 acquisition system connected to a computer. Force, stack voltage, DC voltage (where relevant) and shaker head velocity are measured. The voltages are sensed directly using the SigLab unit, although a voltage divider is used to bring the voltages within range of the acquisition box specifications. The resistance of the measuring branch, totalling 2.8MΩ, is large enough to be neglected in the measurements.

The damper curve is determined separately using the same setup without the piezo stack. It is shown in figure 2. A third order polynomial fit through the origin is performed in order to acquire a function for use in simulations. The jog in the experimental data just above and below zero velocity is attributed to the onset of reversal of the damper displacement leading to stick-slip of the internal seals. For smaller amplitudes this jog maintains a magnitude of 20N making smaller amplitudes less suitable for measurement since this is difficult to simulate accurately.

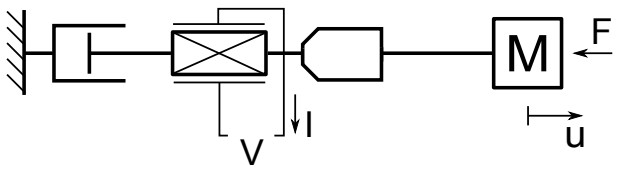

Figure 1: Schematic of experimental setup, left to right: damper, piezo stack, force sensor and shaker

The excitation frequency used is 3Hz. This makes maximum use of the damper without exceeding the force limits of the force sensor and piezo stack. It also allows for a quasistatic approach of the mechan-

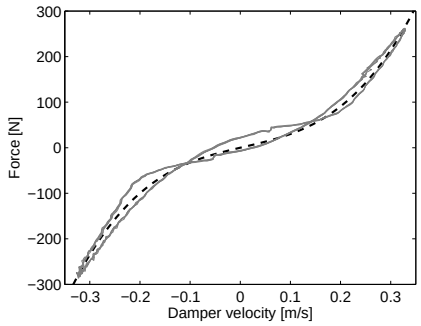

Figure 2: Experimental (grey solid) and fitted (black dashed) damper curve

ical system. From an electrical standpoint, at this frequency the dynamic impedance of the stack is equal to 54kΩ, significantly smaller than the resistance of the measuring system.

Using a piezoelectric stack would imply that the system possesses high electromechanical coupling. Electromechanical coupling denotes the magnitude of the coupling of the two domains. It is normalized such that the value is the ratio of the additional apparent mechanical stiffness resulting from the piezoelectric effect and the mechanical stiffness. The parameter is therefore a direct measure of how much stiffer a system becomes under open circuit conditions. For the stack alone the electromechanical coupling coefficient can be calculated as $k_e^2 = \theta^2 / \left(k_p C_p\right)$. For the stack under consideration this equates to 0.042. Such a value can be considered as high but this is only partly true. Considering the definition by [4] high or low coupling depends also on the ratio of k_e^2 to the dimensionless damping ζ. As an indication assume a damper with a constant viscous damping coefficient of 1000 Ns/m, connecting the maximum values from figure 2 with a straight line. Combined with the mass and stiffness of the setup this yields $\zeta = 0.36$ meaning the damping of the piezoelectric element is negligible.

3. ELECTRONICS

Various circuits are tested: AC Impedance matching (ACIM) [5], DC Impedance matching [4] (DCIM) is used as a baseline comparison and for its insensitivity to the load path, and the SSHI [3] is used to increase the output over the DCIM circuit.

3.1. Open circuit

The piezoelectric coefficient must be determined from an open circuit experiment. Since the system is excited far below resonance θ can be calculated using only the piezoelectric equations instead of performing a compete dynamic analysis:

$$k_p u + \theta V = F \tag{1a}$$

$$\theta u - C_p V = 0 \tag{1b}$$

Rewriting these equations into one and eliminating the displacement u we find the following equation from which θ can be calculated:

$$V_p \theta^2 + F\theta + V_p k_p C_p = 0 \tag{2}$$

This is solved for the positive and negative peaks, yielding four possible values for θ. Only the values near unity are realistic as these coincide best with what is calculated from the material spec.

3.2. AC Impedance matching

For energy dissipation AC impedance matching (ACIM) is considered first. It simply requires a load resistor across the contacts of the piezo element. The circuit possesses an optimal resistance [5] at which the power output is maximized. For a sinusoidal excitation force and low coupling this resistance is $R_{opt} = 1/\left(\omega C_p\right)$. A difficulty in this circuit is that the power harvested depends on the actual load path of the piezo element. As indicated in the previous section the damper curve is approximated using a third order polynomial. This leads to a difference in actuation force between experiment and simulation and a difference in power output is to be expected.

The optimal resistance will also change because of the non-sinusoidal excitation. The damper is nonlinear and changes the RMS value of the force. The two extrema are a step function or a type of pulse function which alternates pulses positive and negative with a zero value in between. The former can be shown to have any optimal resistance up to $2\pi/\left(5\omega C_p\right)$ above which the piezo element has not completely discharged upon strain reversal. The latter requires an infinitely small load to be able to dissipate any power at all within the short time.

Due to these difficulties the maximum dissipated power and optimal resistance are only indicative values and are expected to differ from simulation.

3.3. DC Impedance Matching

The DCIM circuit rectifies the voltage from the piezo stack with a B500R full bridge rectifier and utilizes a large storage capacitor C_s as a buffer to maintain a nearly constant DC voltage, V_{dc}. Figure 3 shows the circuit diagram. The diode rectifier invokes approximately a 1V loss. Equations in this paragraph are found in [4].

The DCIM circuit has two modes of operation. The first is when the piezo element is in open circuit mode

and V_p is alternating from $+V_{dc}$ to $-V_{dc}$ or vice versa. The other is where the piezo element has achieved $\pm V_{dc}$ and conducts through the rectifier.

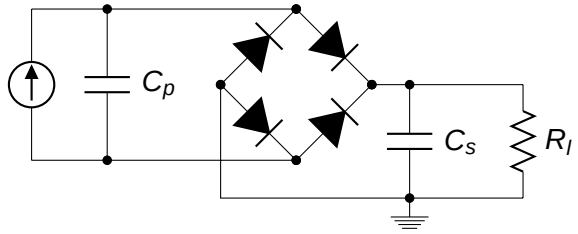

Figure 3: DC Impedance Matching circuit schematic

The main analytical advantage of DCIM is that the power harvested depends only on the extrema of the displacement and the associated frequency. This can be concluded from the derivation by [4] who only consider the values at the start and end of a half cycle. This means that despite the load path not being harmonic, only the peak force values will determine the power harvested. This fact negates the error created by the cubic approximation of the damper in the setup. Using the average values determined from the open circuit approach, simulations are performed using the DCIM circuit and good agreement is expected.

Table 2 summarizes additional parameters for the DCIM circuit. The ideal load resistance for low coupling is $R_{opt} = \pi / \left(2C_p\omega\right)$. The storage capacitance C_s must be chosen sufficiently large to prevent significant oscillations of the DC voltage. In this case C_s is chosen such that at most a 5% drop in voltage occurs in between charge bursts. This is calculated through the standard solution of the first order differential equation which governs the discharge of an RC circuit: $C_s = -\pi / \left(\ln\left(0.95\right)\omega R\right)$. The range of loads is chosen to span one order of magnitude surrounding the optimal resistance. The values shown are corrected for the resistance of the measuring loop and represent the actual loads applied.

Table 2: Additional DCIM settings

	Symbol	Value	Unit
Optimal resistance	R_{opt}	86.8	$[k\Omega]$
Load resistance range	R	26.7-295	$[k\Omega]$
Storage capacitance range	C_s	5-60	$[\mu F]$

3.4. Synchronized Switch Harvesting on Inductor

The Sychronized Switch Harvesting on Inductor (SSHI) circuit [3] is an active circuit. It contains switches and additional components to modify the piezo electric voltage. It requires a small amount of energy from the piezoelectric element to operate. The circuit diagram is shown in figure 4. When compared to the DCIM circuit a switched inductor is added across the contacts of the piezoelectric element. This creates an electrical oscillator with a natural frequency $\omega_{el} = 1/\sqrt{C_p L_1}$, where L_1 is the inductance in Henries [H]. An extensive analysis of the circuit can be found in [6].

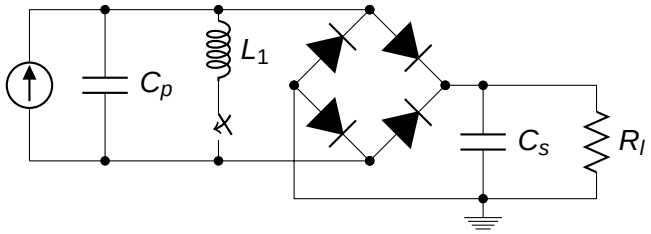

Figure 4: SSHI circuit schematic

Conceptually the SSHI circuit functions by inverting the voltage using the electronic oscillator when a displacement extreme is reached. When the voltage is inverted the oscillator ceases operation. Compared to the DCIM circuit either less time is lost alternating V_p between $\pm V_{dc}$, or a higher V_{dc} can be achieved at a lower resistance. Both situations increase output over the standard DCIM method.

The values of the components used are summarized in table 3 and the switch design is given in figure 5. The remainder of this section describes the design process of the electronics and the determination of these variables. The semiconductor components used are BC560C PNP transistors, 2N7000 MOSFETS and Schottky diodes.

The choice of the inductor value has been investigated extensively in [1]. In this setup the inductor may not be chosen too small to prevent an excessive mechanical impulse following voltage inversion. The resulting vibrations will be damped out and with it a great deal of energy is lost. A similar analysis on this setup shows that $L_1 \geq 5mH$ to prevent these undesired oscillations.

The efficiency of the inductor must also be considered. This is denoted by the quality factor $Q_i = \omega_{el} L_1 / R_{coil}$, with R_{coil} the resistance of the coil. Q_i is equivalent to the mechanical quality factor of a mass-damper-spring system and indicates how little energy is dissipated in one oscillation. A higher value denotes fewer losses.

The inductor quality must be as high as possible at the electrical resonance frequency so that as little energy as possible is lost due to voltage inversion. It is difficult to design inductors of the desired inductance which possess a satisfactory quality factor of at least 10-20: these inductors require ferromagnetic cores. The authors have, until the moment of writ-

ing, not found suitable inductors that do not show significant hysteresis at the required voltage and current. Preliminary experiments have been performed with cored inductors but the hysteresis is so significant that the voltage would drop to zero monotonically instead of oscillate as desired. For the results presented in this paper, a TOKO 181LY-124 100mH inductor is used with DC resistance of 68Ω. At ω_{elec} this yields a quality factor of 4.8.

With the aid of some semiconductor components the switch, which is powered by the piezo element, is capable of tracking the envelope of the piezo voltage. In [7] the layout of the self-powered switch is shown. In [8] a clear explanation is given of the functioning of the switch. An envelope capacitor C_e follows V_p and closes the switch when the voltage falls below the envelope voltage V_e. The piezo voltage then begins to oscillate but after one half cycle the reverse direction is blocked by a diode. In reality, the single switch in figure 4 is replaced by two such switches in parallel, connected with reversed polarity. Each switch accomplishes inversion for only one direction.

Another consideration is the use of the NPN transistor in the switching circuit. For low current and voltage levels it is an excellent solution. As the amount of switched power begins to increase the switch begins to consume excessive amounts of power due to the way transistors function. A switched current must be matched with a smaller control current. This is what drives the size of the envelope capacitor. Also, the larger the transistor the smaller the ratio between switched and control current. A smaller current ratio further increases the required C_e.

For this application the switched power and current is sufficiently large to warrant the use of a MOSFET. This device requires a threshold voltage across the control and switched ports (gate, and drain/source ports) to allow conduction through another channel. This penalty is significant for low voltage signals. Although the MOSFET based switch does not switch immediately following the peak piezo voltage, it consumes far less energy in doing so because no current is necessary through the gate. Therefore, following preliminary experimentation and different from [7], the NPN transistor is replaced with a 2N7000 MOSFET. The circuit diagram of this modified switch is shown in figure 5.

4. RESULTS

All experiments described in this section were performed in one session after the damper temperature had stabilized under excitation. This was done to obtain the best practical comparison between the circuits. A typical result for the developed force is shown in figure 6. The result is asymmetric, presumably due

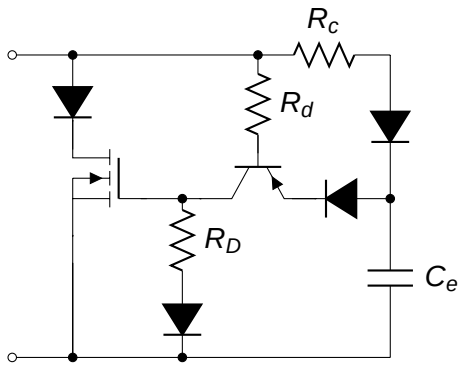

Figure 5: Self powered circuit layout

Table 3: Additional SSHI settings

	Symbol	Value	Unit
Inductance	L_1	100	[mH]
Inductor resistance	R_{coil}	68	[Ω]
Load resistance range	R	0.1-1	[MΩ]
Storage capacitor	C_s	1-20	[μF]
Envelope capacitance	C_e	22	[nF]
Charge resistance	R_c	22	[kΩ]
PNP base resistor	R_d	470	[kΩ]
MOSFET Gate-source resistor	R_D	470	[kΩ]

to variations in the damper. The variation in developed force showed no trend over time and remained within 2% of the average value for all measurements.

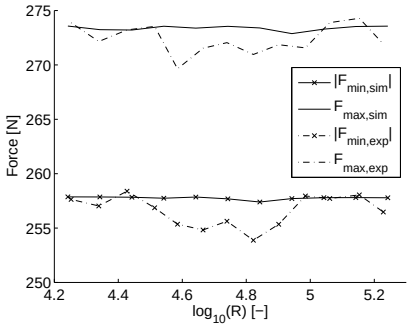

Figure 6: Maximum and minimum force values resulting from simulation and experiment

Using a measurement as in figure 7 it is possible to calculate θ using equation 2. This resulted in a value of 1.05 N/V, as shown in table 1.

The results of the ACIM experiment are plotted in figures 8 and 9. The power does not only show a difference in harvested power but also in the optimal resistance.

The difference in optimal resistance is in part due to the non-sinusoidal excitation, as discussed in section 3. The aforementioned optimal value is calculated assuming a sinusoidal excitation. Here the root mean square of the force signal is lower than for a sine wave, indicating a shorter time in which the

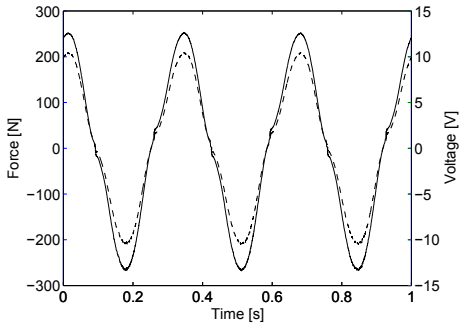

Figure 7: Force (solid, left axis) and voltage (dashed, right axis) waveforms for open circuit conditions

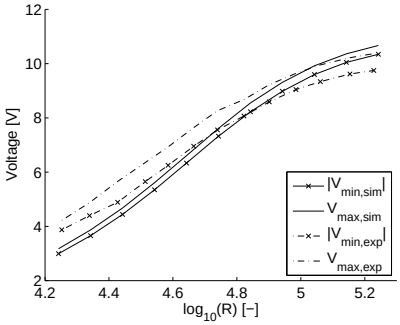

Figure 8: ACIM voltage amplitude

power can dissipate in the resistor. The experiment agrees with the expectations.

The results for DCIM are shown in figures 10 and 11. Again the experiment shows better performance than the simulation (22% higher) and a shift in the optimal resistance value (24% lower). Neither of these were expected.

Concluding with the SSHI, figure 12 shows the resulting force and voltage waveforms. It can be seen that the inversion commences after the force –and therefore stack displacement– has reached an extreme value. The 2V decrease is visible after which nearly 50% inversion efficiency is achieved. This implies an inductor quality of only 2.1. Note that the voltage appears to invert quicker than before a 2V drop, this can mostly be attributed to transition effects accelerating the switching process, once the FET begins to conduct.

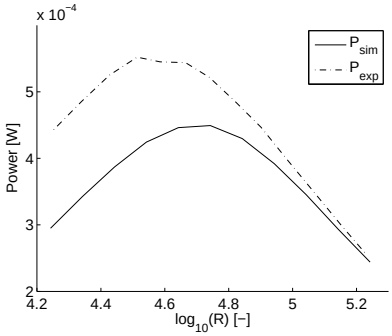

Figure 9: ACIM average power output

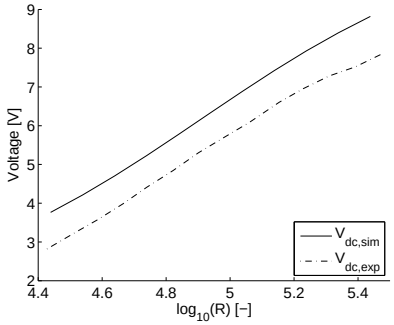

Figure 10: DCIM output voltage

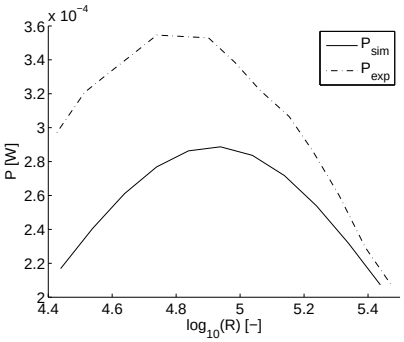

Figure 11: DCIM average power output

In the simulation the experimentally determined inductor quality is used. Figure 13 shown is the inversion quality for the various experiments. It is taken from the extrema surrounding the respective inversion action so the 2V loss due to the MOSFET is included in the calculation. Figures 14 and 15 show the DC voltage and power results. Contrary to the AC and DC experiments here the experiment falls short compared to simulation.

5. DISCUSSION

The experiments of the previous section showed mixed results. The ACIM and DCIM circuits showed consistent differences with simulation, giving confidence in the developed models. The power is consistently higher and the optimal resistance lower. For the ACIM circuit both were expected. For the DCIM

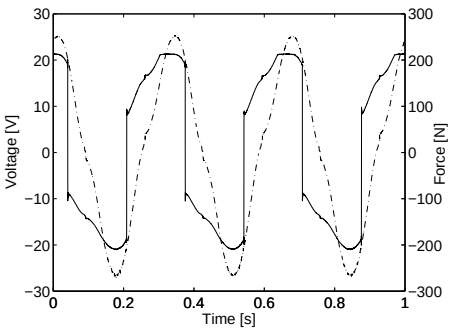

Figure 12: Applied force (dashed, right vertical axis) and piezo voltge V_p (solid, left axis)

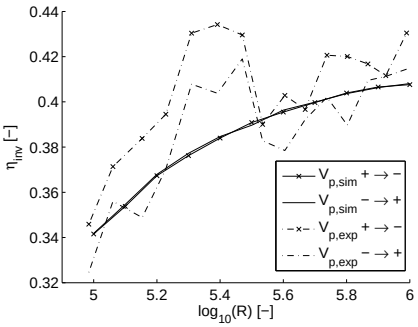

Figure 13: Voltage inversion efficiency

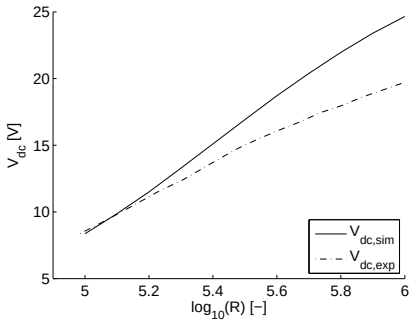

Figure 14: SSHI DC voltage results

circuit neither was anticipated due to the lower sensitivity to non-sinusoidal excitation.

In light of [9] an analysis of the piezo stack was done using a Keithley 4200 Semiconductor Characterization System. It demonstrated variations of up to 15% in the DC capacitance of the stack within the operating bounds of the experimental setup. It is safe to assume that the piezoelectric coupling θ may also show some variation, greatly increasing the uncertainty of the simulation. A technically more advanced and stable material should be used for future validation. Considering the non-linearities in the piezo material (capacitance and presumably coupling) and the damper a 20% difference between simulation and experiment is reasonable.

Based on [1] it was anticipated that the SSHI circuit would yield 3-4 times more power than the DCIM circuit. Here only a factor of 2 was achieved. Although simulations matched reasonably well with experiment, this was only after modifying the quality factor of the inductor in the simulation. Using the original inductor value of 4.5, 1.5mW of power was anticipated. The inductor exhibits more hysteresis than the DC resistance implied. Clearly more research is required to find a suitable inductor for this circuit and even more so for a full scale system where the currents are larger. This appears to be the largest hurdle in developing this concept.

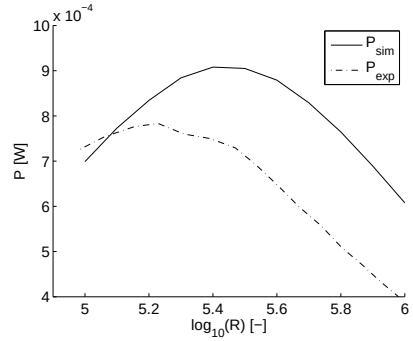

Figure 15: SSHI power results

The SSHI circuit functioned well from an operational standpoint. Using the MOSFETS as opposed to the NPN transistors inversion effiency was improved. With a suitable inductor minimal losses would be incurred by the circuit as the MOSFET requires a voltage and no current to function. The required C_e is only a few percent of the piezo capacitance. For the transistor based circuit the envelope capacitor C_e –upwards of 10% of C_p– and resistors R_d and R_D values must be calculated precisely to match the inductor current. For these experiments the transistor based circuit achieved only $\sim$25% inversion efficiency.

The less than satisfactory inversion efficiency of the MOSFET switch can also in part be attributed to the voltage penalty incurred by the FET. Compared to the voltage amplitude of 20V this should however decrease the efficiency by 5-10% at most. Based on literature 45% is by no means an excellent value, [10, 11] show far better results reaching 70-80%.

In [12] the importance of the inductor quality is clearly emphasized. With force or voltage constraints being absent a well designed inductor can increase the output of an SSHI system over tenfold over the DCIM circuit. This is assuming a displacement driven system which is the case for the lag damper, the excitation is quasi-static. In [2] it was shown that the lag damper in combination with the SSHI circuit may drive the stack voltage up far enough to damage the material. However a significant increase in output over the DCIM circuit is still possible.

When compared to [1] a different piezo material was used. Being soft PZT, the stack used in the experiments can handle less voltage and stress than hard PZT. Another strange phenomenon can be found in figure 12. The voltage peaks are of different shape. The positive peak shows a flat spot, clearly indicating that the rectifier is conducting. The negative peak does not show a significant plateau and detailed inspection of the results show only a very brief conduction period. This may be due to the non-linearity of the capacitance and a possible non-linearity in the piezoelectric parametrs θ.

Many improvements are to be made in this setup, both in terms of circuitry and materials in order to match that performance. In [1], a specific output of 47mJ/cm^3 per cycle was found from simulation and

here only 1.4mJ/cm^3 per cycle. Using a good inductor $Q_i > 10$ and achieving an inversion efficiency of 80% can increase the output by a factor of 2. The hard material can also handle over twice the voltage of this soft PZT. Moreover, the maximum allowed voltage of the piezo material was not achieved in this setup. With harvested power being proportional to the square of the voltage this implies a fourfold increase. There is much room for improvement.

6. CONCLUSIONS AND RECOMMENDATIONS

Experiments were conducted to validate simulations concerning a piezoelectrically augmented lag damper. Its purpose is to provide power for in blade health monitoring systems which aid in increasing the technical lifespan of rotor blades.

Validation was only partially successful. Despite strong non-linearities in the various components, simulations of passive circuits showed reasonable agreement with experimentation with at most 20% difference in key results. On the other hand the active SSHI circuit could not be validated as well, falling short of the simulation results in [1]. Considering the decent match of the passive circuit this is presumably due to the electrical circuit not being tuned properly and to non-linear problems in the inductors used. Further research should be conducted in this direction to find suitable inductors.

The piezo stack used in this setup was an off-the-shelf component. Minimal consideration was given to the material properties, therefore a material was used with lesser performance that what was considered in [1]. A new series should be conducted with the material considered in aforementioned paper after the inductor issue has been addressed.

7. ACKNOWLEDGEMENTS

Many thanks go to Mickaël Lallart for continued communication concerning the SSHI circuit self powered switch.

This project is funded by the Clean Sky Joint Technology Initiative (grant number [CSJU-GAM-GRC-2008-001]9) - GRC1 Innovative Rotor Blades, which is part of the European Union's 7th Framework Program (FP7/2007-2013).

References

[1] P. H. de Jong, A. de Boer, R. Loendersloot, and P. J. M. van der Hoogt. Power harvesting in a helicopter lag damper. In *ERF*. ERF, September 2011.

[2] P. H. de Jong, A. de Boer, R. Loendersloot, and P. J. M. van der Hoogt. Power harvesting in a helicopter rotor using a piezo stack in the lag damper. *Journal of Intelligent Materials Systems and Structures*, 2012.

[3] A. Badel, D. Guyomar, E. Lefeuvre, and C. Richard. Piezoelectric energy harvesting using a synchronized switch technique. *Journal of Intelligent Material Systems and Structures*, 17, 2006.

[4] Y. C. Shu and I. C. Lien. Efficiency of energy conversion for a piezoelectric power harvesting system. *Journal of micromechanics and microengineering*, 2006.

[5] S. Roundy. On the effectiveness of vibration based energy harvesting. *Journal of Intelligent Material Systems and Structures*, 2005.

[6] Y. C. Shu, I. C. Lien, and W. J. Wu. An improved analysis of the sshi interface in piezoelectric energy harvesting. *Smart Materials and Structures*, 16:2253–2264, 2007.

[7] M. Lallart and D. Guyomar. An optimized self-powered switching circuit for non-linear energy harvesting with low voltage. *Smart Materials and Structures*, 2008.

[8] J. Liang and W-H Liao. Improved design and analysis of self-powered synchronized switch interface circuit for piezoelectric energy harvesting systems. *IEEE Transactions on indstrial electronics*, 59(4), 2012.

[9] G. Yang, Z. Yue, Y. Ji, and L. Li. Dielectric nonlinearity of stack piezoelectric actuator under the combined uniaxial mechanical and electric loads. *Journal of Applied Physics*, 104, 2008.

[10] M. Lallart, E. Lefeuvre, C. Richard, and D. Guyomar. Self-powered circuit for broadband, multimodal piezoelectric vibration control. *Sensors and Actuators, a Physical*, 2007.

[11] A. Badel, D. Guyomar, E. Lefeuvre, and C. Richard. Efficiency enhancement of a piezoelectric energy harvesting device in pulsed operation by synchronous charge inversion. *Journal of Intelligent Material Systems and Structures*, 16, 2005.

[12] E. Lefeuvre, A. Badel, C. Richard, L. Petit, and D. Guyomar. A comparison between several vibration-powered piezoelectric generators for standalone systems. *Sensors and Actuators A: Physical*, 126:405–416, 2006.